International Journal of Thermal Sciences 49 (2010) 131–142

Contents lists available at ScienceDirect

International Journal of Thermal Sciences

journal homepage: www.elsevier.com/locate/ijts

MRT-Lattice Boltzmann simulation of forced convection in a plane channel with an inclined square cylinder

M.A. Moussaoui [a], M. Jami [a], A. Mezrhab [a,*], H. Naji [b]

[a] Laboratoire de Mécanique & Energétique, Département de Physique, Faculté des sciences, Université Mohamed 1, Oujda, Maroc, Morocco
[b] Laboratoire de Mécanique de Lille UMR 8107 CNRS/Université Lille 1 – Sciences et Technologies/Polytech'Lille/, F-59655 Villeneuve d'Ascq cedex, France

ARTICLE INFO

Article history:
Received 24 January 2009
Received in revised form
19 June 2009
Accepted 25 June 2009
Available online 18 July 2009

Keywords:
Lattice Boltzmann equation
Finite difference method
Heat transfer
Laminar channel flow
Square cylinder
Numerical simulation
Forced convection

ABSTRACT

Numerical investigation of the two-dimensional flow and heat transfer, in a horizontal channel differentially heated and obstructed by an inclined square cylinder mounted to the approaching flow with an angle of inclination equal to 45° is carried out. The strategy is based on the combination of the Multiple Relaxation Time Lattice Boltzmann Equation (*MRT-LBE*) to obtain the velocities and on the Finite Differences Method (*FDM*) to solve the equation of energy. This numerical scheme is assessed against previous publications. Close attention is paid to Reynolds number ranging from 0 to 300 at Prandtl number, $Pr = 0.71$ with constant physical properties of the fluid. Results are presented in terms of streamline contours, isotherms, drag coefficient, Strouhal number, local and average Nusselt numbers for various Reynolds numbers. The computed results show that the presence of such bluff body affects significantly the fluid flow and causes enhancement in the heat transfer from the hot bottom wall to the flow.

1. Introduction

For a long time, the study of flow past bluff bodies such as square and circular cylinders has fascinated researchers because of the intrinsic complexities and importance of these flows in many industrially important applications, obvious examples are cooling of electronic components, cooling towers, oil and gas pipelines, heat exchanger systems, chimneys, and flow-meters. In spite of appearances, the fluid flowing over blocks displays a complicated unsteady motion and presents a good opportunity to understand these fundamental mechanisms of unsteady flow interactions occurring in various technologies. Among the many studies achieved on this topic and available in literature, we cite the work of Davis et al. [1] who have performed experimental and numerical investigations of flow around a rectangular cylinder placed in a horizontal channel with the Reynolds number ranging from 100 to 2000 and two values of the blockage ratio, $\beta = 1/6$ and $\beta = 1/4$. They have discussed the effects of the variations of Reynolds number, rectangle aspect ratio, blockage ratio and upstream velocity profile upon the forces acting on the rectangle and the structure of the wake. Strouhal numbers obtained both computationally and experimentally are compared for two values of the blockage ratio. Igarashi [2] conducted an experimental study of the flow characteristics around a square prism at an angle of attack ($0° \le a \le 45°$) in the range of sub-critical Reynolds numbers. He concluded that for $a < 15°$, the perfect separated regime may be subdivided into symmetric and asymmetric flows, particularly at $a = 5°$. For $15° < a < 35°$, the lower separated shear layer reattaches and a separation bubble exists on the lower surface. For $35° < a < 45°$, the flow field resembles one about a wedge. In another work [3], he studied the local as well as the average heat transfer from a square prism to an air stream in the range of sub-critical Reynolds number. He has observed that the average heat transfer has a minimum value at an angle of attack (a) equal to 12°–13° and a maximum value at $a = 20°$–$25°$.

Numerically, Li and Humphrey [4] have performed the modeling of unsteady, two-dimensional flow and heat transfer due to a square cylinder located asymmetrically between the parallel sliding walls of a channel at various orientations. Their numerous investigations showed that the presence of the bounding walls in the flow, affected significantly the behavior of vortex shedding behind the body. Sohankar et al. [5] studied confined flow over a square cylinder at incidence ($a = 0°$–$45°$) to investigate the influence of the Reynolds number and the angle of incidence on the Strouhal number, the lift, the drag and base suction coefficients. Turki et al. [6] have numerically investigated the mixed convection from a horizontal square

* Corresponding author. Tel.: +212 536500601/02; fax: +212 536500603.
E-mail addresses: mezrhab@fso.ump.ma, amezrhab@yahoo.fr (A. Mezrhab).

1290-0729/$ – see front matter © 2009 Published by Elsevier Masson SAS.
doi:10.1016/j.ijthermalsci.2009.06.009

Nomenclature

C_f	dimensionless skin friction coefficient, Eq. (3)
C	local skin friction coefficient, ReC_f
C_d	drag coefficient, Eq. (1)
C_l	lift coefficient, Eq. (2)
d	square cylinder diagonal height, m
f	dominant frequency, s^{-1}
F_D	total force per unit length on the cylinder in the streamwise direction, $N\,m^{-1}$
F_L	total force per unit length on the cylinder in the cross-stream direction, $N\,m^{-1}$
g	acceleration of gravity, $m\,s^{-2}$
H	channel height, m
L	length of the channel, m
Nu	local Nusselt number, $(d\theta/dy)_{y=0}$
$\overline{Nu}$	space-averaged Nusselt number
$\langle\overline{Nu}\rangle$	space- and time-averaged Nusselt number
Pr	Prandtl number, ν/α
Re	channel Reynolds number, $u_{max}d/\nu$
Re_c	Critical Reynolds number
St	Strouhal number, fd/u_{max}
T	temperature, K
$\boldsymbol{u}$	flow velocity, $\boldsymbol{u}(u,v)$
u	x-velocity component, $m\,s^{-1}$
u_{max}	maximum velocity at the inlet, $m\,s^{-1}$
U	dimensionless x-velocity component
v	y-velocity component, $m\,s^{-1}$
x, y	Cartesian coordinates, m
X, Y	dimensionless Cartesian coordinates, $X=x/L$, $Y=y/L$
X_{in}	distance of the blocks from the inlet, m

Greek symbols

α	thermal diffusivity, $m^2\,s^{-1}$
β	blockage ratio, d/H
ΔT	maximal temperature difference, $T_h - T_c$, K
μ	dynamic viscosity of fluid, $kg\,m^{-1}\,s^{-1}$
ν	kinematic viscosity of the fluid, $m^2\,s^{-1}$
ρ	density of fluid, $kg\,m^{-3}$
θ	dimensionless temperature, $(T-T_c)/\Delta T$

Acronyms

BGK	Bhatnagar-Gross-Krook
CFD	Computational Fluid Dynamics
D2Q9	2-D 9-velocity
FDM	Finite Difference Method
LBE	Lattice Boltzmann Equation
LGM	Lattice Gas Model
MRT	Multiple Relaxation Time
SRT	Single-Relaxation Time

Subscripts

c	cold
f	fluid
h	hot
w	wall

cylinder to air for $62 \le Re \le 200$ and Richardson number (Ri) up to 0.1 for a blockage ratio of 1/4 and 1/8. The value of the critical Reynolds number (onset of periodic flow) decreases while the Strouhal number increases with increasing the Richardson number. They also proposed correlations for the Nusselt number at different values of the Richardson number ($Ri = 0$, 0.05 and 0.1). Abbassi et al. [7] carried out a numerical investigation using control volume method with the Simpler algorithm for pressure–velocity coupling to study the forced convection in a horizontal channel with a built-in triangular prism. They found that for symmetric flow corresponding to a lower Reynolds numbers ($Re < 45$), the presence of the triangular prism has only a local weak effects on the heat transfer from the channel and on the flow pattern, while in periodic flow ($Re \ge 45$), heat transfer from the channel is seen to increase strongly in presence of the triangular prism. De and Dalal [8] developed a second-order accurate finite volume code with a non-staggered arrangement of variables employing momentum interpolation for the pressure–velocity coupling for two-dimensional laminar flow and heat transfer past a triangular cylinder placed in a horizontal channel. Their results, presented for the range of $80 \le Re \le 200$ and blockage ratio $1/12 \le \beta \le 1/3$, showed that the Strouhal number and rms of lift coefficient increase significantly with blockage ratio and Reynolds number while the overall Nusselt number remains almost constant for different blockage ratios. At lower blockage ratios, the flow is found to be similar to the unconfined flow and is more prone to wake instability.

It is worth noting that most of the numerical studies available in the literature employed techniques based on solving the Navier–Stokes equation. However, it is not easy to deal with problems of complex geometries or when there are several fluid phases or several fluids. In this context a different approach, namely Lattice Boltzmann Equation (LBE) has found extensive applications in simulating physical phenomena of various complexities. The LBE emerges as a simple, innovative, viable and efficient alternative to the traditional CFD methods. Significant advances of theoretical algorithms and practical industrial applications of the LBE approach have been made (see for example, Ginzburg et al. [9,10]) where a Lattice Boltzmann method, with just two relaxation times, is used to improve the algorithm with respect to BGK operator. By now, some of the advantages in this fundamentally new alternative method have been considerably more understood and appreciated in the mainstream scientific and engineering communities. These advantages include: Less numerical dissipations due to the linear and Lagrange type advection operator in the Boltzmann equation, local dynamic interactions allowing highly parallel computations, physical control of boundary conditions for complex hydrodynamic fluxes on arbitrary geometries, microscopically consistent realization of thermodynamics and intrinsic handling of interface properties in multiphase flows, and simpler yet more faithful formulation of complex macroscopic physical properties in a wider range of scales. The embedded advantages of LBE have created a great opportunity to apply this innovative approach to real engineering problems encountered in a variety of industries. The LBE has been widely used in many kinds of complex flows such as single component hydrodynamics, multiphase and multi-component fluids, magneto-hydrodynamics, reaction-diffusion systems, flows through porous media and turbulent flows (see Chen and Doolen [11], Mezrhab et al. [12], Semma et al. [13]).

Cheng et al. [14] have used a lattice Boltzmann method to investigate a linear shear flow past a square cylinder at low Reynolds number. Their results show that the vortex structure behind the cylinder is strongly shear-rate dependent. However, the study was limited to a single Reynolds number. Zhou et al. [15] carried out a numerical study on reduction of fluid forces acting on a square cylinder in two-dimensional channel using a control plate; they used the Lattice Boltzmann technique and their results showed that

the drag and the fluctuating lift are significantly reduced by the presence of the control plate.

It is well known that the vortex shedding phenomenon can be dramatically altered for uniform flows past a bluff body at different Reynolds numbers. Of course, the vortex structure behind an obstacle in shear flow may also be Reynolds-number dependent. Breuer et al. [16] investigated in detail the confined flow around a square bar mounted inside a plane channel with a blockage ratio of 1/8 by two entirely different numerical techniques, namely a Lattice Boltzmann Equation (LBE) and a finite volume method (FVM). They found an excellent agreement between LBE and FVM. Guo et al. [17] conducted a comparative study of the Lattice Boltzmann equation (LBE) and the Gas-Kinetic Scheme (GKS) methods for 2D incompressible laminar flows past a square block symmetrically placed in a channel with the Reynolds number between 10 and 300. Their results show that both LBE and GKS methods yield to quantitatively similar results for laminar flow simulations, and agree well with existing ones, provided that a sufficient grid resolution is given. For 2D problems, the LBE is about 10 and 3 times faster than the GKS for steady and unsteady flow calculations, respectively, while the GKS uses less memory. Guo et al. [18] studied the confined flow around a square cylinder mounted inside a two-dimensional channel (blockage ratio $\beta = 1/8$) by using a non-uniform Lattice BGK model. They presented a detailed analysis for a range of Reynolds numbers between 1 and 500 and showed that the model gives accurate results for complex flows. The mechanism of heat transfer under such an unsteady flow in a channel flow with the insertion of a cylinder has not been investigated to the same extent.

The main purpose of the present work is to study the effect of the presence of an inclined square cylinder on the fluid flow and heat transfer into two-dimensional channel differentially heated, for which the Reynolds number ranges from 20 to 300. The investigation is carried out using a hybrid scheme with Thermal Lattice Boltzmann and Finite Difference method. This scheme was proposed by Lallemand and Luo [19,20] and by Mezrhab et al. [21], and was used by many authors, as an example, we can quote Leemput et al. [22] and Van Treeck et al. [23].

The remainder of this paper is organized as follows. Section 2 presents the problem under investigation and gives a concise introduction of the numerical scheme (MRT-LBE). In Section 3, results from MRT-LBE simulation are presented and discussed. Also, in this section, onset of vortex shedding, steady and periodic flow description and wake visualization are dealt with separately in order to make the current investigation clear. Finally, we conclude the paper with a summary of our results in Section 4.

2. Formulation of flow problem

2.1. Statement of the problem

The test case chosen for the present study is the two-dimensional laminar flow past an a square cylinder inclined of 45 degrees with respect to the channel centerline and symmetrically placed inside a channel, as depicted in Fig. 1. The fluid circulating in the channel is the air ($Pr = 0.71$) and its physical properties, except its density, are supposed to be constant. The ratio L/d is set equal to 30.75 and the blockage ratio is $\beta = d/H$=1/4. The cylinder is placed at a distance $X_{in}/d = 8$ downstream from the inlet section of the channel. Values of L/d and X_{in}/d are those reported by Davis et al. [1]. The inclined square cylinder, the top wall and the incoming stream are assumed to be in a constant cold dimensionless temperature $\theta_c = -0.5$, while the bottom wall is at a hot dimensionless temperature $\theta_h = 0.5$.

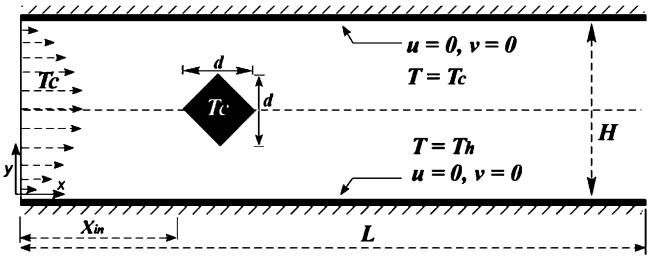

Fig. 1. Schematic configuration with built-in inclined square cylinder.

At the inlet, a fully developed parabolic profile for the streamwise is enforced; at the outlet, an artificial open boundary condition (OBC) is imposed, so, the Neumann boundary condition (NBC) is used, i.e., the streamwise gradients of the velocity and temperature are set to zero. Note that with this condition, we avoid having to use a large computational domain.

The viscous and pressure forces acting on the cylinder were used to calculate the drag and lift coefficients (C_d, C_l). These coefficients are defined as:

$$C_d = \frac{F_D}{0.5\rho u_{max}^2 d} \tag{1}$$

$$C_l = \frac{F_L}{0.5\rho u_{max}^2 d} \tag{2}$$

where F_D and F_L are the drag and lift forces exerted by the fluid on the cylinder, respectively. As the force on the cylinder caused by the viscous is too small, all forces mentioned herein refer to the force induced by the pressure distribution, which were obtained by integration.

The dimensionless skin friction coefficient is given by:

$$C_f = 2(\partial U/\partial Y)_w/\mathrm{Re} \tag{3}$$

2.2. Multiple relaxation time Lattice Boltzmann equation (MRT-LBE)

The Lattice Boltzmann Equation (LBE) is a numerical scheme evolved from the Lattice Gas Model (LGM) in order to overcome the difficulties encountered with the LGM [24]. In LBE, the fluid field is discretized by a group of microscopic particles. The density distributions of these particles perform two types of motions: collision and streaming. In what follows, we use the D2Q9 model (see Fig. 2) on a square lattice with lattice spacing $\delta x = \delta y$ (where D refers to space dimensions and Q to the number of particles at a computational node). Each node comprises three kinds of particles, rest

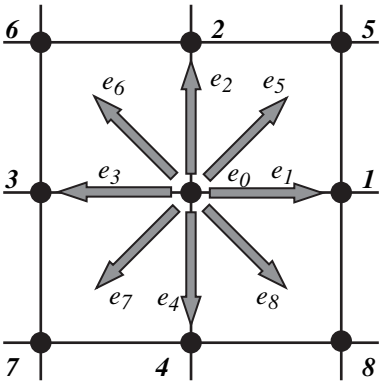

Fig. 2. A 2-D 9-velocity lattice (D2Q9) model.

particles that reside in the nodes of the lattice, particles that move along the coordinate directions and particles that move along diagonal directions.

The simplest Lattice Boltzmann equation (LBE) is the lattice Bhatnagar-Gross-Krook (BGK) equation based on a single-relaxation time (SRT) approximation [25]. Due to its extreme simplicity, the lattice BGK equation has become the most popular lattice Boltzmann model. However, this simplicity comes at the expense of numerical instability [26] and inaccuracy in implementing boundary conditions [27]. These deficiencies in the BGK models can be overcome with the use of multiple relaxation-time (MRT) model introduced by d'Humières [28]. It has been clearly demonstrated that the LBE models with MRT collision operators have inherent advantages over their BGK counterparts [25,26]. The MRT-lattice Boltzmann equation (also referred to as the generalized lattice Boltzmann equation (GLBE) or the moment method) overcomes some obvious defects of the BGK model, such as fixed Prandtl number ($Pr = 1$ for the BGK model) and fixed ratio between the kinematic and bulk viscosities. The MRT-LBE models are much more stable than the BGK, since the different relaxation times can be individually tuned to achieve "optimal" stability [26].

For a MRT-LBE model with 9 velocities, a set of velocity distribution functions $f_i(r_j, t_n)$, $i \in \{0, \ldots, 8\}$ is defined on each node r_j of the lattice and for time t_n. The evolution equation for the MRT-LBE of 9 velocities on a 2-dimensional lattice $r_j \in (\delta_x \mathbb{Z})^2$ with discrete time $t_n \in \delta_t \mathbb{N} = \delta_t\{0, 1, 2, \ldots\}$ is:

$$\boldsymbol{f}(\boldsymbol{r_j} + \boldsymbol{e}_i\delta_t, t_n + \delta_t) - \boldsymbol{f}(\boldsymbol{r}_j, t_n) = -M^{-1}S(\boldsymbol{m}(\boldsymbol{r}_j, t_n) - \boldsymbol{m}^{\mathrm{eq}}(\boldsymbol{r}_j, t_n)) \tag{4}$$

where $\boldsymbol{f}(\boldsymbol{r},t)$, $\boldsymbol{m}(\boldsymbol{r},t)$ and $\boldsymbol{m}^{\mathrm{eq}}(\boldsymbol{r},t)$ are 9-dimensional vectors for the distribution functions, the moments, and the equilibria of moments, respectively, e.g., $\boldsymbol{f} = (f_0, f_1, \ldots, f_8)^T \in \mathbb{V}(= \mathbb{R}^9)$, and $\boldsymbol{m} = (m_0, m_1, \ldots, m_8)^T \in \mathbb{M}(= \mathbb{R}^9)$, T being the transport operator. M is the 9×9 transformation matrix such that $\boldsymbol{m} = M\boldsymbol{f}$ and $\boldsymbol{f} = M^{-1}\boldsymbol{m}$ and S is the collision matrix in the moment space M. Explicitly, matrices M and S of the incompressible lattice Boltzmann model can be written as, respectively:

$$M = \begin{pmatrix} 1 & 1 & 1 & 1 & 1 & 1 & 1 & 1 & 1 \\ -4 & -1 & -1 & -1 & -1 & 2 & 2 & 2 & 2 \\ 4 & -2 & -2 & -2 & -2 & 1 & 1 & 1 & 1 \\ 0 & 1 & 0 & -1 & 0 & 1 & -1 & -1 & 1 \\ 0 & -2 & 0 & 2 & 0 & 1 & -1 & -1 & 1 \\ 0 & 0 & 1 & 0 & -1 & 1 & 1 & -1 & -1 \\ 0 & 0 & -2 & 0 & 2 & 1 & 1 & -1 & -1 \\ 0 & 1 & -1 & 1 & -1 & 0 & 0 & 0 & 0 \\ 0 & 0 & 0 & 0 & 0 & 1 & -1 & 1 & -1 \end{pmatrix} \tag{5}$$

and

$$S = \mathrm{diag}(0, s_1, s_2, 0, s_4, 0, s_6, s_7, s_8) \tag{6}$$

where s_i are relaxation rates.

The nine-velocity square lattice model, which is often referred to as the 2-D 9-velocity (D2Q9) model (Fig. 1), has been widely and successfully used for simulating two-dimensional (2-D) flows. In the D2Q9 model, $\boldsymbol{e}_i$ denotes the discrete velocity set, namely,

$$\boldsymbol{e}_i = \begin{cases} (0,0), & i = 0 \\ (\cos[(i-1)\pi/2], \sin([(i-1)\pi/2]))c, & 1 \le i \le 4 \\ \sqrt{2}c(\cos[(2i-9)\pi/4/], \sin([(2i-9)\pi/4/])), & 5 \le i \le 8 \end{cases} \tag{7}$$

where $c = \delta_x/\delta_t$ is the particle velocity and δ_x and δ_t are the lattice grid spacing and the time step, respectively. From here on, we shall use the units of $\delta_x = \delta_t = 1$ such that all the relevant quantities correspond are dimensionless.

The nine components of the moment vector $\boldsymbol{m}$ are arranged in the following order: $m_0 = \rho$ is the fluid density, $\boldsymbol{m}_1 = e$ is related to energy, $\boldsymbol{m}_2 = \varepsilon$ is related to the energy square, $m_{3,5} = j_{x,y}$ are components of the momentum $J = (j_x, j_y)$, $m_{4,6} = q_{x,y}$ are related to components of the energy flux and $m_{7,8} = p_{xx,xy}$ are related to the components of the symmetric and traceless strain rate tensor. These nine moments are separated into two groups: (ρ, m_3, m_5) are the conserved moments which are locally conserved in the collision process; (m_1, m_2, m_4, m_6, m_7, m_8) are the non-conserved moments. In the MRT-LBE framework, all modes (i.e., moments) are orthogonal and their relaxation rates can be controlled individually. This allows the MRT model to include the maximum number of adjustable parameters. Following, the non-conserved quantities are calculated from the relaxation equations:

$$m_j^{ac} = (1 - s_j)m_j^{bc} + s_j m_j^{\mathrm{eq}} \tag{8}$$

where m_j^{ac} denote the moments after collision, m_j^{bc} are the post-collision moments, s_j are the inverse relaxation times which are the diagonal elements of the matrix S and m_j^{eq} are the corresponding equilibrium moments. Note that the collision rates s_0, s_3 and s_5 are not relevant, since they are related to the conserved moments. In order to obtain a consistent dynamics viscosity, relaxation rates s_7 and s_8 have to be equal $s_7 = s_8$. The other relaxation rates have no physical meaning for incompressible flows and stability reasons, they can be freely chosen in the range $0 < s_i < 2$.

In the lattice units of $\delta_x = \delta_t = 1$, the speed of sound in this model is $c_s = c/\sqrt{3}$ and the kinematic viscosity ν is given by:

$$\nu = c_s^2\delta_t\left(\frac{1}{s_7} - \frac{1}{2}\right) = c_s^2\delta_t\left(\frac{1}{s_8} - \frac{1}{2}\right) \tag{9}$$

The equilibrium values of the non-conserved moment $\boldsymbol{m}^{\mathrm{eq}}$ are chosen to be [21]:

$$\begin{aligned} e^{\mathrm{eq}} &= -2\rho + 3\left(j_x^2 + j_y^2\right), \quad \varepsilon^{\mathrm{eq}} = \rho - 3\left(j_x^2 + j_y^2\right)\Big/\rho_m \\ q_x^{\mathrm{eq}} &= -j_x, \quad q_y^{\mathrm{eq}} = -j_y \\ p_{xx}^{\mathrm{eq}} &= \left(j_x^2 - j_y^2\right)\Big/\rho_m, \quad p_{xy}^{\mathrm{eq}} = j_x j_y/\rho_m \end{aligned} \tag{10}$$

The constant ρ_m is the mean density in the system and is usually set to be unity in simulations.

The Boltzmann equation is linked to the equations of macroscopic hydrodynamics by averaging properties over velocity space such that the macroscopic density, ρ, and momentum, $\rho\boldsymbol{u}$, are given by

$$\rho = \sum_{i=0}^{8} f_i \tag{11}$$

$$\rho\boldsymbol{u} = \boldsymbol{J}\left(j_x, j_y\right) = \sum_{i=0}^{8} f_i\boldsymbol{e}_i \tag{12}$$

The bounce-back condition is applied at all walls [29]. This type of boundary condition locates the physical wall at the half grid spacing beyond the last fluid node (see Fig. 3). On the interface

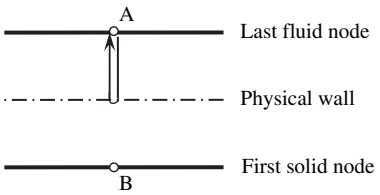

Fig. 3. Bounce-back boundary condition on each direction.

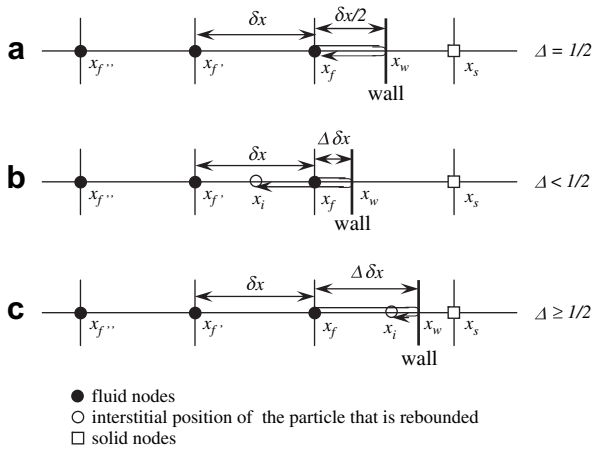

Fig. 4. Schematic for the interpolation procedure of boundary conditions.

between the fluid and the sides of the inclined square prism, we have used a combination of the bounce-back scheme and spatial interpolations of second order because there are some particles that are going to be in interstitial positions after being rebounded.

2.2.1. Boundary conditions

In this subsection, we describe the interpolation procedure which is depicted in Fig. 4. The usual bounce-back condition [30] is applied at all solid walls which are located at the half grid spacing beyond the last fluid node x_f. In cases where walls are arbitrary located, a simple boundary condition based on the bounce-back scheme and a spatial quadratic interpolation [29,31] is used. In Fig. 4, the parameter Δ represents the fraction in the fluid region of a grid spacing intersected by the boundary, i.e., $\Delta = |x_f - x_w|/\delta_x$. Fig. 4(a) shows that the particle moves from x_f toward x_w, then it comes back to its place after being reflected by the wall. This case is subjected to the usual bounce-back boundary conditions. Whereas in the two others cases (Fig. 4(b) and (c)), the particle stands in interstitial positions x_i. To keep the structure of the grid, the distribution had to be reconstructed. For example: in case of $\Delta < 1/2$, at time t, the distribution function of the particle with velocity pointing to the wall (Fig. 4(b)) at the grid point x_f (a fluid node) would end up at the point x_i located at a distance $(1-2\Delta)\delta x$ away from the grid point x_f, after the bounce-back collision. Because x_i is not a grid point, the value of f_3 at the grid point x_f needs to be reconstructed. Noticing that f_1 starting from point x_i would become f_3 at the grid point x_f after the bounce-back collision with the wall, the values of f_1 at the point x_i are built using a quadratic interpolation which requires values of f_1 at three points that are $f_1(x_f)$, $f_1(x'_f) = f_1(x_f - e_1)$ and $f_1(x''_f) = f_1(x_f - 2e_1)$. For the case where $\Delta \geq 1/2$, $f_3(x_f)$ is constructed by a quadratic interpolation involving $f_3(x_f)$ that is equal to $f_1(x_f)$ before the bounce-back collision, and the values of f_3 at the nodes after collision and advection, i.e., $f_3(x'_f)$, and $f_3(x''_f)$. It is emphasized that this method needs to treat the boundary conditions separately for $\Delta < 1/2$ and $\Delta \geq 1/2$. In other words, interpolations are performed as follows:

1. For $\Delta < 1/2$, interpolate before propagation and bounce-back collision.
2. For $\Delta \geq 1/2$, interpolate after propagation and bounce-back collision.

This is done in order to avoid the use of extrapolations in the boundary conditions for the sake of numerical stability. This leads to the following interpolation formulas (where the notations $\widehat{f}_i$ and f_i denote the post-collision distribution functions before and after advection):

$$f_i\left(x_f,t\right) = \Delta(1+2\Delta)\widehat{f}_i\left(x_f,t\right) + \left(1-4\Delta^2\right)\widehat{f}_i\left(x'_f,t\right) - \Delta(1-2\Delta)\widehat{f}_i\left(x''_f,t\right) \text{ for } \Delta < 1/2 \tag{13}$$

$$f_{\bar{i}}\left(x_f,t\right) = \frac{1}{\Delta(1+2\Delta)}\widehat{f}_i\left(x_f,t\right) + \frac{(2\Delta-1)}{\Delta}f_{\bar{i}}\left(x_{f'},t\right) - \frac{(2\Delta-1)}{(2\Delta+1)}f_{\bar{i}}\left(x''_f,t\right) \text{ for } \Delta \geq 1/2 \tag{14}$$

where $f_{\bar{i}}$ is the distribution function of the velocity $e_{\bar{i}} \equiv -e_i$. Note that, if one uses an efficient LBE code in which collisions and motions are performed together, then the information needed in the previous equations are moved one step along e_i and so the effect of boundaries is taken care of by:

$$f_{\bar{i}}\left(x_f,t\right) = \Delta(1+2\Delta)f_i\left(x_f+e_i,t\right) + \left(1-4\Delta^2\right)f_i\left(x_f,t\right) - \Delta(1-2\Delta)f_i\left(x_f-e_i,t\right) \tag{15}$$

$$f_{\bar{i}}\left(x_f,t\right) = \frac{1}{\Delta(1+2\Delta)}f_i\left(x_f+e_i,t\right) + \frac{(2\Delta-1)}{\Delta}f_{\bar{i}}\left(x_f-e_i,t\right) - \frac{(2\Delta-1)}{(2\Delta+1)}f_{\bar{i}}\left(x_f-2e_i,t\right) \tag{16}$$

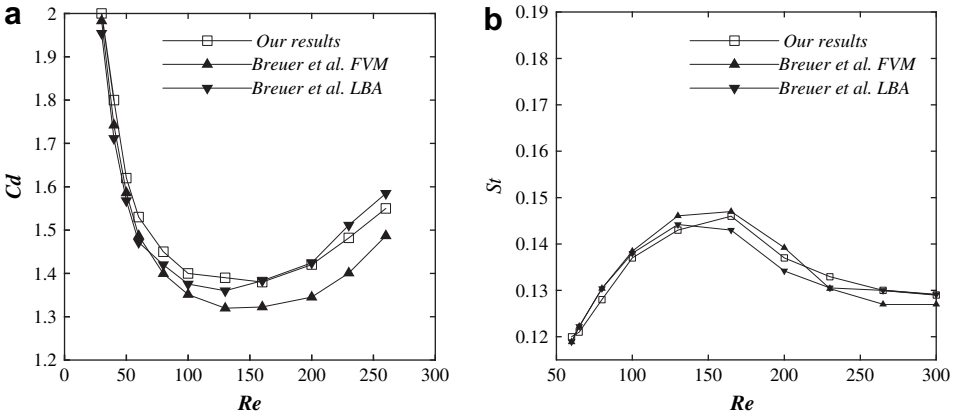

Fig. 5. Comparison with previous work for: (a) the drag coefficient, (b) Strouhal number.

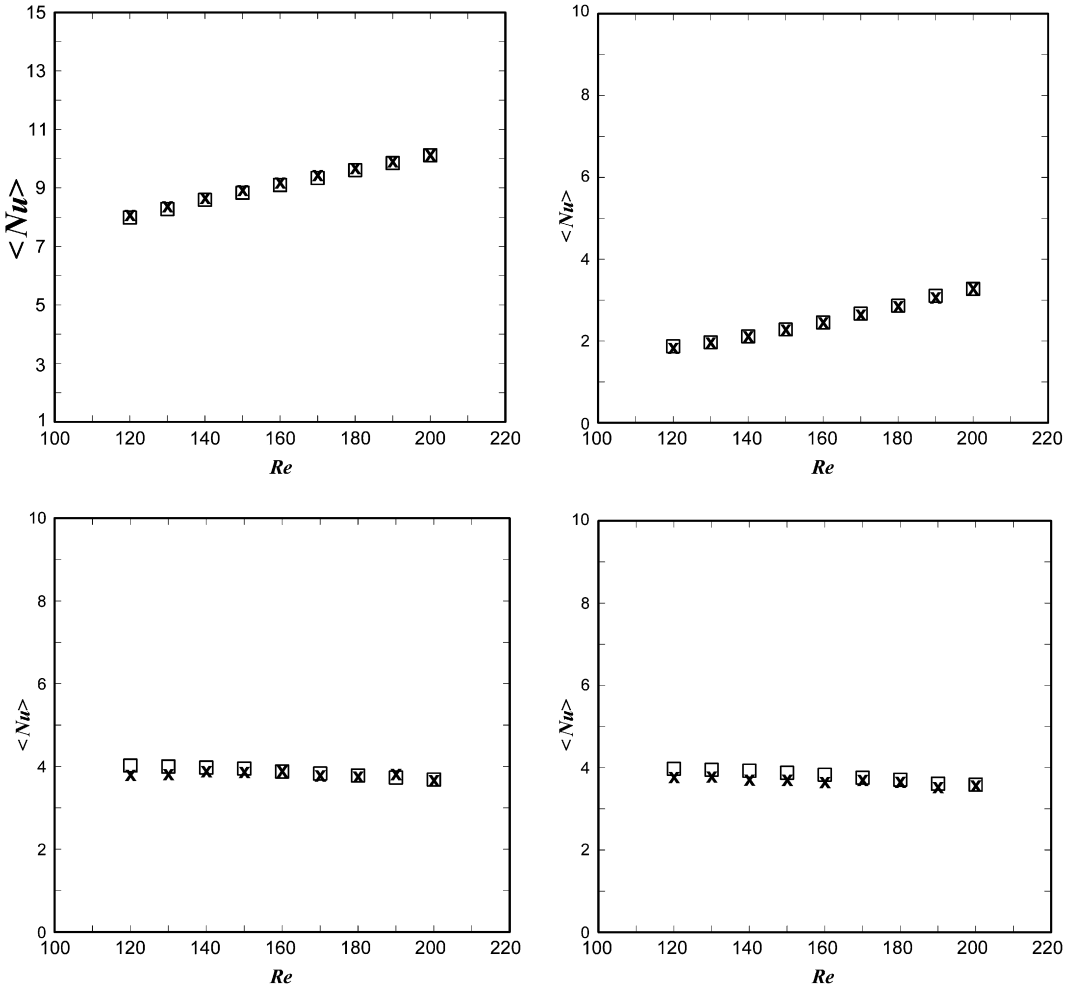

Fig. 6. Variation of space- and time-averaged *Nusselt* number versus *Re* on each face of the cylinder. *x*: our results, □: Turki et al. [6].

2.3. Equations of temperature

As we use the LBE approach for the fluid flow, we could have used a second LBE model (with just one conserved quantity of scalar character) to compute the temperature. However, the corresponding computational cost is the almost the same as the fluid LBE. For this reason, we have chosen to use here the simple finite difference approach since it reduces the computational cost of the temperature by a factor of the order of 5. The energy equation is given by the following:

$$\frac{D\theta}{Dt} = \alpha_f \nabla^2 \theta \tag{17}$$

where $D/Dt = \partial/\partial t + u_j \partial/\partial x_j$ denotes the convective derivative.

Table 1
Results for grid test for $Re = 200$.

Mesh	*d* (pts)	C_d	*St*	$\langle \overline{Nu} \rangle$
953×123	31	21,368	02,100	1.859
1261×163	41	20,944	02,097	1.840
1567×203	51	20,611	02,101	1.830
1875×243	61	20,373	02,104	1.828

To solve the energy equation, we use the finite difference scheme and we take the same grid points as for the LBE scheme, Mezrhab et al. [21].

Let us consider the space and temporal step equal to 1, the equation (17) is solved explicitly using a first-order forward difference scheme in time (Equation (18)) and a second-order central difference scheme (Equations (19) and (20)) for space discretization as follows:

$$\frac{\partial \theta}{\partial t} \approx \theta^{n+1}(i,j) - \theta^{n}(i,j) \tag{18}$$

$$\frac{\partial \theta}{\partial x} \approx \frac{\theta(i+1,j) - \theta(i-1,j)}{2}, \quad \frac{\partial \theta}{\partial y} \approx \frac{\theta(i,j+1) - \theta(i,j-1)}{2} \tag{19}$$

$$\frac{\partial^2 \theta}{\partial x^2} \approx \theta(i+1,j) - 2\theta(i,j) + \theta(i-1,j),$$

$$\frac{\partial^2 \theta}{\partial y^2} \approx \theta(i,j+1) - 2\theta(i,j) + \theta(i,j-1) \tag{20}$$

2.4. Nusselt number

The Nusselt number, which is of a greater interest in engineering applications, is computed to provide an idea on the heat transfer

characteristics. The Nusselt number can be defined as the local temperature gradient as follows:The local Nusselt number (Nu) based on obstacle height is evaluated as:

$$Nu = -\frac{\partial\theta}{\partial Y} \tag{21}$$

The thermal heat transferred from the hot wall to the flow is characterized by the space-averaged Nusselt number evaluated as follows:

$$\overline{Nu} = \int_0^1 -\frac{\partial\theta}{\partial Y}dX \tag{22}$$

The space- and time-averaged Nusselt number is given by:

$$\langle\overline{Nu}\rangle = \frac{1}{\tau_2-\tau_1}\int_{\tau_1}^{\tau_2}\overline{Nu}d\tau \tag{23}$$

where the time interval $(\tau_2-\tau_1)$ is the period of oscillation of the space-averaged Nusselt number $\overline{Nu}$.

3. Results and discussion

Numerical simulations are performed to examine the influence of the inclined square obstacle upon the flow and temperature field inside the channel. In particular, the effects of the Reynolds number on Strouhal number, time-averaged drag coefficient, local Nusselt number and space- and time-averaged Nusselt number are

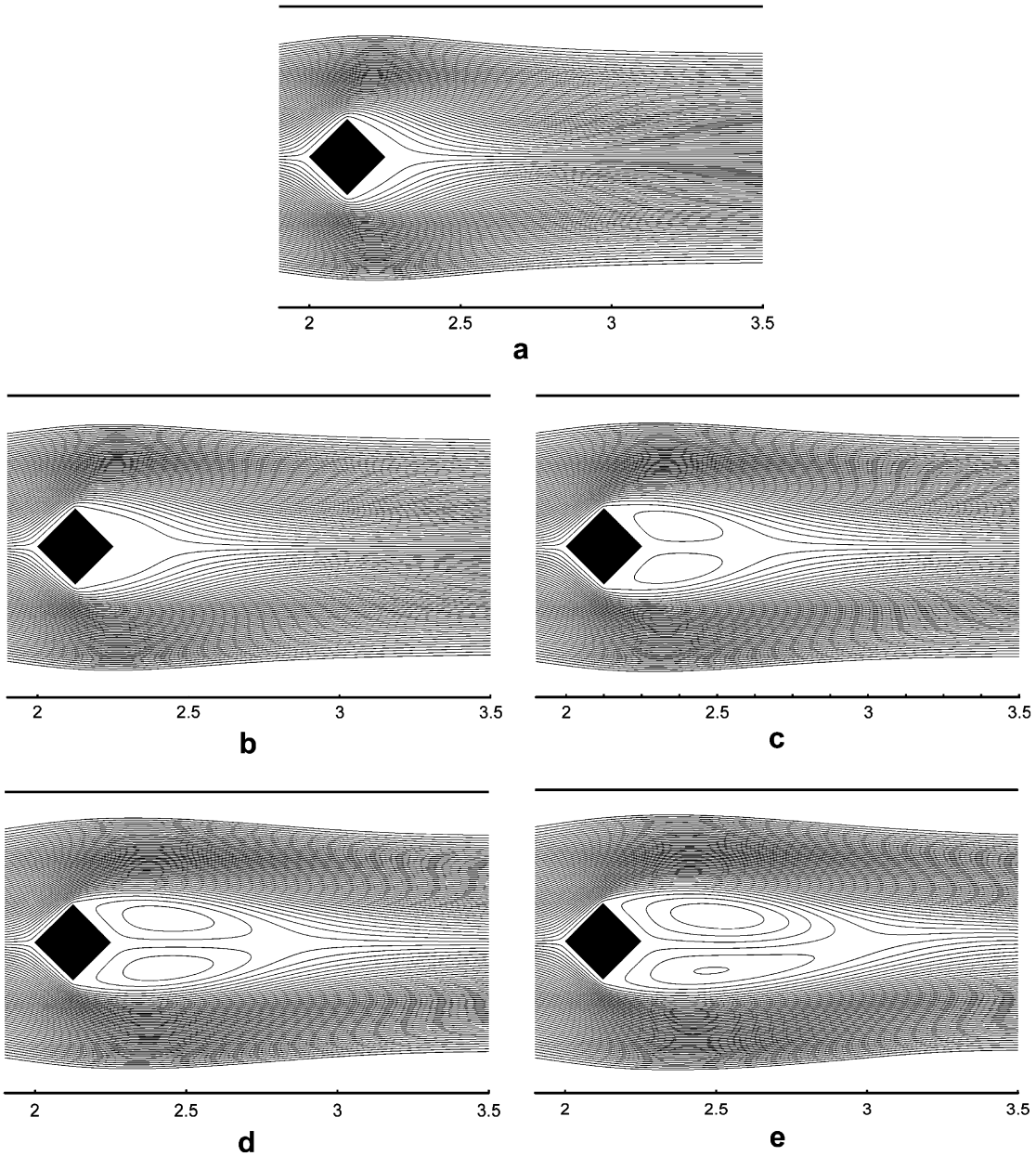

Fig. 7. Streamlines: (a) $Re = 10$, (b) $Re = 20$, (c) $Re = 40$, (d) $Re = 60$, (e) $Re = 80$.

investigated. It should be noted that for the periodic flow, all solutions are dependent on time, then, in the following study curves and streamline fields are given at an arbitrary instant.

3.1. Code validation

The code based on the (MRT-LBE / FDM) was extensively exercised on benchmark problems to check its validity (see Mezrhab et al. [12,21]; Jami et al. [32]). In this paper, we have chosen to present the code validation for two studies. Firstly, computations were performed for the configuration studied by Breuer et al. [16] who have modeled a confined flow around a cylinder with square cross-section mounted inside a plane channel with a blockage ratio of 1/8. We present in Fig. 5(a) and (b), the time-averaged drag coefficient and the Strouhal number for different values of the Reynolds number *Re* ranged between 10 and 250. It should be noted that the present results are compared with the ones reported by Breuer obtained from the Finite Volume Method (FVM) using 560×340 non uniform grids and the Lattice Boltzmann Automata (LBA) using 2000×320 uniform grids. As can be seen, our results compare favourably graphically with those reported by Breuer et al. [16]. Secondly, our results were validated with those obtained by Turki et al. [6]. An unsteady flow field and heat transfer characteristics in horizontal channel with a built-in heated square cylinder with blockage ratio equal 1/4 is considered. The variations of the time-averaged Nusselt number versus Reynolds number on each side of the square cylinder are compared in Fig. 6 with those obtained by Turki et al. [6] for different Reynolds numbers. Also here, an excellent agreement is noted between our results and those obtained by Turki et al. [6].

A preliminary study was carried out to determine the optimum grid. To check the grid independence, different computations were performed for $Re = 200$ and for different uniform grids ($Nx \times Ny$). To do this, we have considered four progressively meshes, namely 953×123, 1261×163, 1567×203 and 1875×243 where the number of grid nodes distributed over a diagonal of the cylinder is 31, 41, 51 and 61, respectively. From Table 1, one can deduce that the maximum difference between the values of C_d, St and $\langle \overline{Nu} \rangle$ obtained for the 1567×203 grid and the finest 1875×243 grid was less than 1.17%, 0.14% and 0.11%, respectively. Therefore, for a better compromise between the accuracy of results and the calculation time, the grid of 1567×203 points was chosen for all simulations reported in this paper.

In the following, numerical results obtained with air as a working fluid ($Pr = 0.71$) are presented and discussed.

3.2. Streamlines and isotherms

Fig. 7 shows the structure of the wake downstream of the obstacle for different Reynolds numbers ranging from 10 to 80. The effect of Reynolds number on the flow pattern and the structure of the steady recirculation eddies is clearly observed. For very low Reynolds number characterized by the combined effects of low velocity and high viscosity, the creeping steady flow past the inclined square cylinder persists without separation. As *Re* increases, the magnitude of viscous forces decreases until a certain value, at which separation of the laminar boundary layers occurs. As consequence, the wake comprises a steady recirculation region of two symmetrically placed vortices on each side of the wake that rotate in opposite directions, as shown in Fig. 7(c–e). The length of these vortices grows as *Re* increases. The streamline profiles are plotted at different axial locations in the channel, and still symmetric with respect the oncoming flow. For $Re = 80$ (see Fig. 7(e)), the symmetrical behaviours observed behind the obstacle begins to be destroyed, but the recirculation region is still observed. For $Re > 80$ and for a critical Reynolds number, the fluid flow changes its behaviour and the wake loses its original symmetry. An unsteady flow takes place and a repeating pattern of swirling vortices caused by the unsteady separation flow over the obstacle is now observed. This periodic state of the flow pattern is characterized by the alternate shedding vortices from the rear face of the inclined square cylinder into the stream. This phenomenon, well known as the von Karman vortex streets, is visualized by a representative instantaneous streamline contours in Fig. 8(a–c).

In the periodic state, $Re \geq Re_c$, and as the Reynolds number increases, the oscillations in the wake grow in magnitude, and this state begins to shed vortices into the stream. The unsteadiness in the flow increases with Reynolds number. Just behind the rear half of the obstacle, the separation occurs while producing two small vortices. These vortices grow slowly with the increase of *Re*. For this

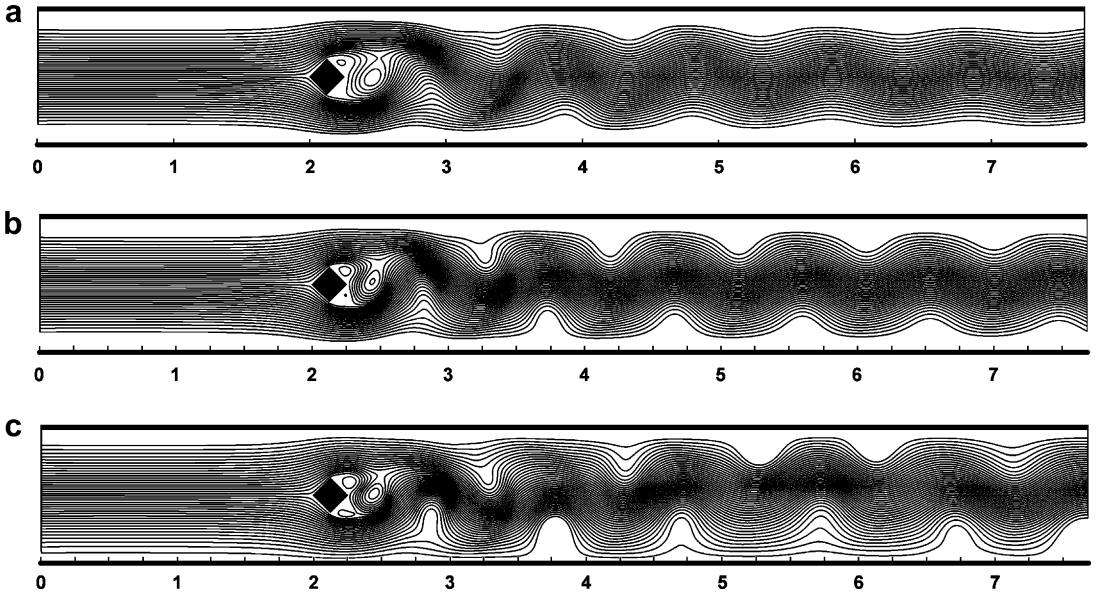

Fig. 8. Streamlines: (a) $Re = 100$, (b) $Re = 200$, (c) $Re = 300$.

study the critical Reynolds number is found to be $Re_c \approx 82$. As mentioned by Sohankar et al. [5], it may be conjectured that the critical Reynolds number characterizing the onset of vortex shedding increases with increasing blockage.

Patterns of isotherms for various Reynolds numbers are shown in Fig. 9(a–f). From these figures, one can conclude that the increase of *Re* has a beneficial effect on the heat transfer from the hot wall to the flow. For $Re \leq 80$, (Fig. 9(a–c)), the thickness of the thermal layer adjacent to the hot bottom wall decreases as *Re* increases. For these values of *Re*, the flow is symmetrical and characterized by a vertical gradient of temperature across the channel. The presence of the inclined square cylinder has only a local effect and does not grossly distort the isotherms and streamlines.

When the flow becomes asymmetric (Fig. 9(d–f)), the heat transfer from the hot wall to the flow is more influenced by the presence of the inclined square cylinder. In fact, the thermal boundary layer is greatly disturbed by the periodic flow caused by the obstacle, and isotherms are removed far away and tend to be convected toward the top plate proving hence that the medium flow is more heated in asymmetric flow than in symmetric flow.

3.2.1. Drag coefficient and Strouhal number

One of the most important parameters for flow around an obstacle is the drag coefficient C_d. Fig. 10 depicts the time-averaged drag coefficient C_d against Reynolds number *Re*. In the region of small *Re* numbers the drag coefficient varies strongly with *Re*. In fact, in the steady state ($0 \leq Re \leq 80$), due to diminishing effect of viscous force, the drag coefficient decreases with increase of *Re* until a local minimum $C_{dmin} = 1.783$ where *Re* reaches its critical value. In the unsteady 2D flow regime ($82 \leq Re \leq 300$), the near-wake becomes instable and a sinusoidal oscillation starts. The averaged C_d increases slightly with the increasing of *Re*. This can be attributed to the streamlined shape of the inclined square cylinder which facilitates formation of a thin boundary layer on the surfaces facing the incoming flow.

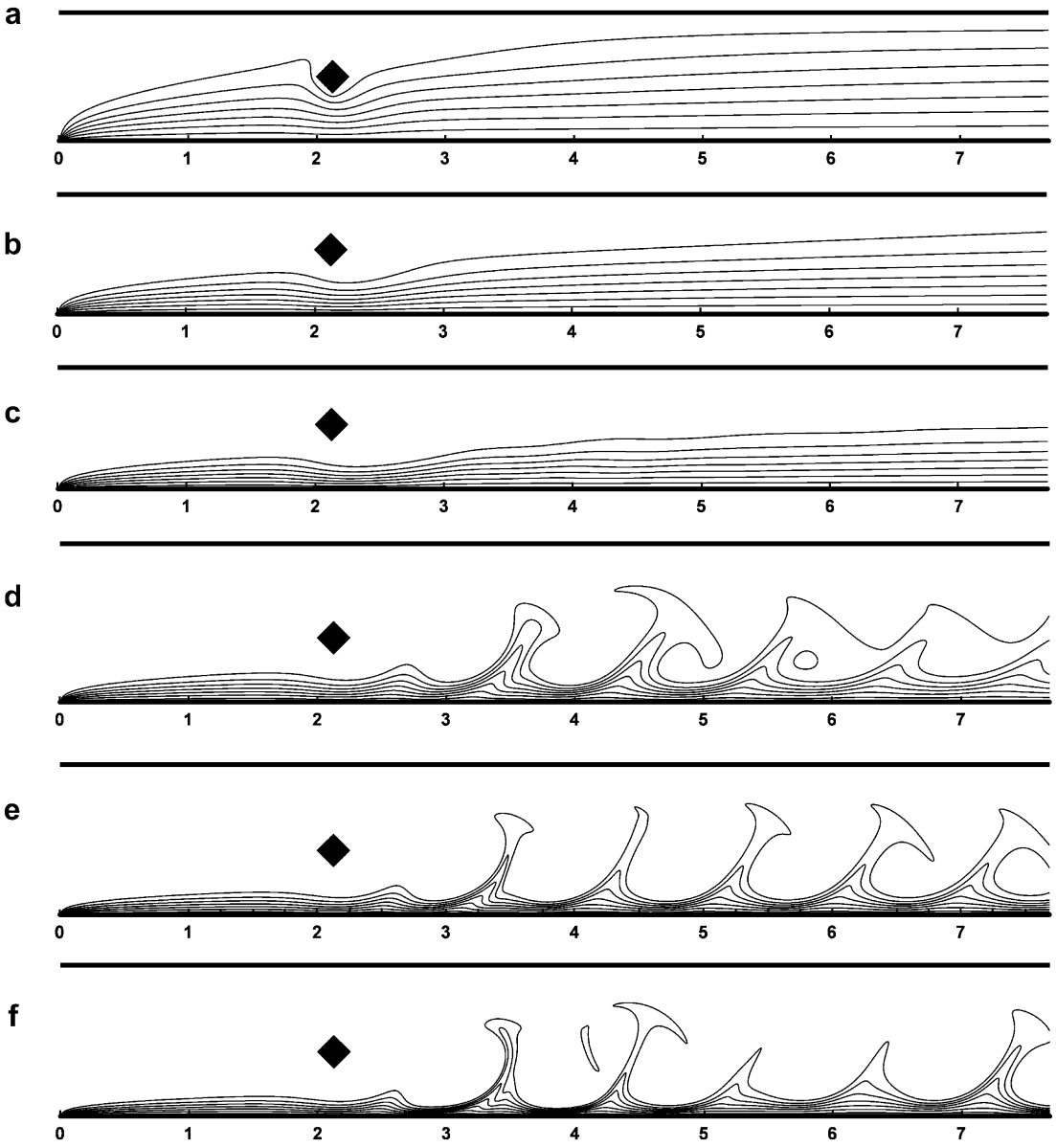

Fig. 9. Isotherms: (a) $Re = 10$, (b) $Re = 40$, (c) $Re = 80$, (d) $Re = 100$, (e) $Re = 200$, (f) $Re = 300$.

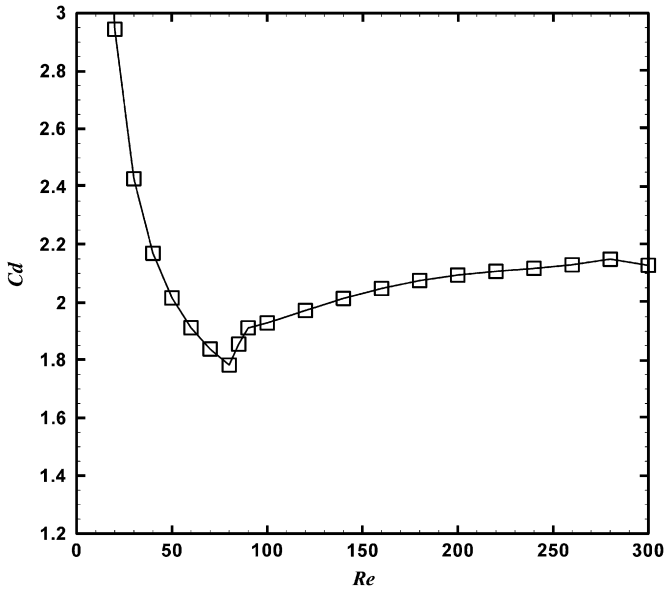

Fig. 10. Time-averaged drag coefficient versus *Re*.

Another important quantity in unsteady periodic flow is the vortex shedding frequency, which is determined by the Strouhal number defined by fd/u_{max}, f being the frequency of vortex shedding. The Strouhal Number represents a measure of the ratio of inertial forces due to the unsteadiness of the flow or local acceleration to the inertial forces due to changes in velocity from one point to another in the flow field. *St* has been determined from the time evolution plot of the lift coefficient distribution by calculating the time period for one cycle of vortex shedding. Once the time period is known, the corresponding frequency and then the Strouhal number can be evaluated. Note that the characteristic frequency f can be also determined by a spectral analysis (fast Fourier transformation FFT) of time series of the lift coefficient. Fig. 11 summarizes the variation of the computed Strouhal number against Reynolds number. Note that the Strouhal number was calculated from the time history of the lift coefficient. The frequency of vortex shedding increases almost linearly with *Re* which is prolonged to $Re/Re_c \approx 2$. This behaviour was observed by Kahawita and Wang [33] in their computations for trapezoidal bluff bodies, and the same observation was found by De et al. [34] for a triangular cylinder. Further increase in *Re* causes the curve to increase at a slower rate until it reaches a flat maximum around $Re = 200$. After that, the frequency of shedding falls down. This interesting behaviour was also observed in the experiments of Okajima [35].

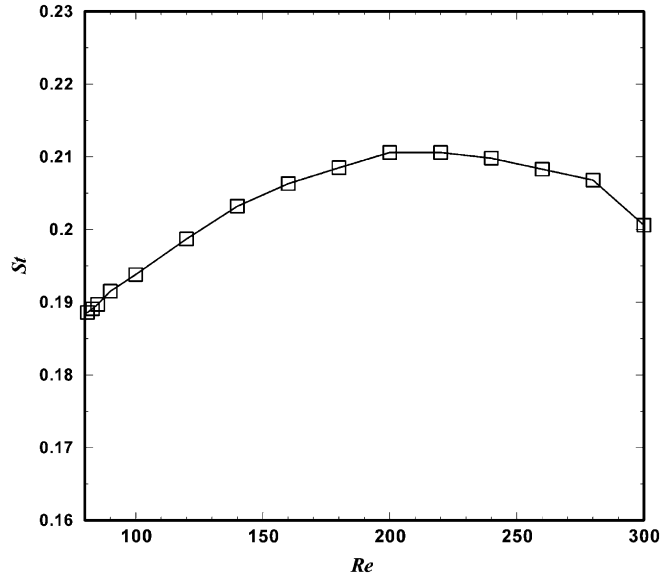

Fig. 11. Strouhal number versus *Re*.

3.2.2. Skin friction

It is well known that the enhancement in heat transfer is associated with penalty in terms of increased skin friction coefficient leading to higher pressure drop. The local skin friction coefficient for the two channel walls in the presence of the inclined square cylinder is presented in Fig. 12 for two different Reynolds numbers ($Re = 50, 150$).

At $Re = 50$ (symmetric flow), the coefficient C for the two walls is symmetric about the value $C = 0$. This result is expected because the symmetrical flow behaves by the same manner near the two plates. The presence of the inclined square obstacle involves increased value of surface friction on the channel walls (in absolute value) to a peak located at $X_{in} + d/2$, due to the acceleration of the flow. Thereafter, it decreases due to deceleration and tends toward its asymptotic value in fully developed flow. At $Re = 150$ (periodic flow), a complete change of the behavior of C is observed. The curves become instantaneously waved along the two walls behind the obstacle with decrease amplitude when we move away from the obstacle. These regions of high skin friction are created by the sweep motion due to streamwise vortices.

3.2.3. Local Nusselt number

Local bottom wall Nusselt number in the presence and in the absence of the inclined square cylinder for $Re = 50$ and $Re = 150$ is shown in Fig. 13. In the inlet region, a thermally developing flow exists, and all curves show nearly identical behavior. In the absence of the obstacle, the Nusselt number is very higher near $y = 0$ and decreases monotonically until reaching the channel exit. At $Re = 50$, when the flow is steady, *Nu* increases immediately after the

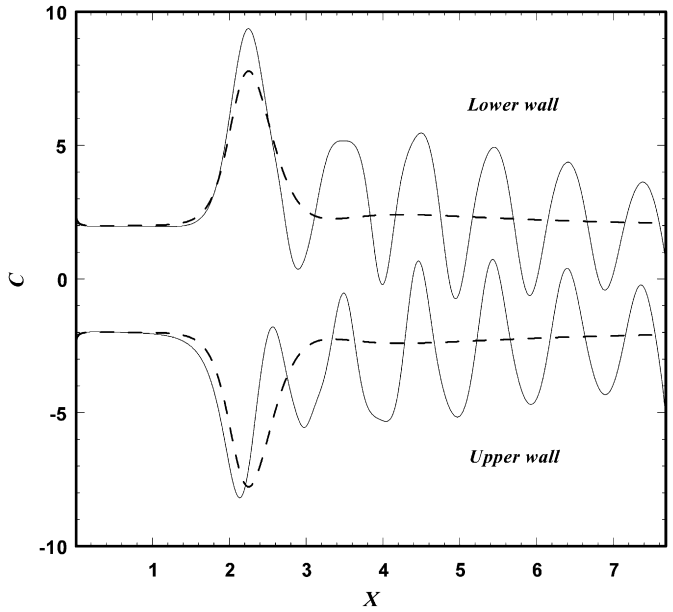

Fig. 12. Variation of skin friction on the channel walls: dashed line: $Re = 50$; Solid line: $Re = 150$.

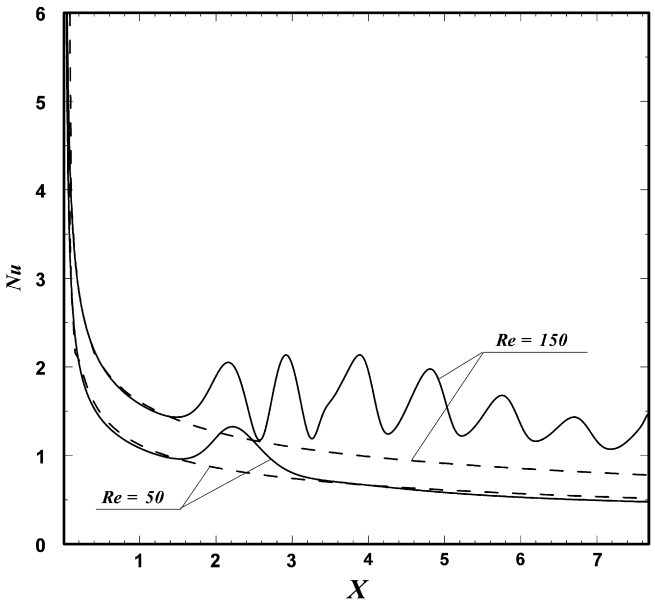

Fig. 13. Local Nusselt number distribution along the lower wall. Dashed line: without obstacle; solid line: with obstacle.

location of the inclined square obstacle, as one moves from the cylinder and after attaining a maximum value, it decreases in the far wake. This maximal value of *Nu* corresponds approximately to the reattachment point at the back of the obstacle. Thus, the presence of the obstacle has just a little local effect by increasing slowly the local Nusselt number and only one peak appears. In contrast, at $Re = 150$, the effect of the presence of the inclined square prism is more important. The *Nu* curve is well disturbed, but appears floating above the dashed line because the vortex shedding after the inclined square cylinder is unsteady. Secondary peaks and crest further downstream occur. At the exit region and for $Re = 150$, the asymptotic *Nu* value is found to be higher when the obstacle is present. An immediate conclusion can be made: the periodic flow promotes the heat transfer from the hot plate to the near flow, and this heat is immediately advected and diffused by the Von Karmen street vortex to the medium flow.

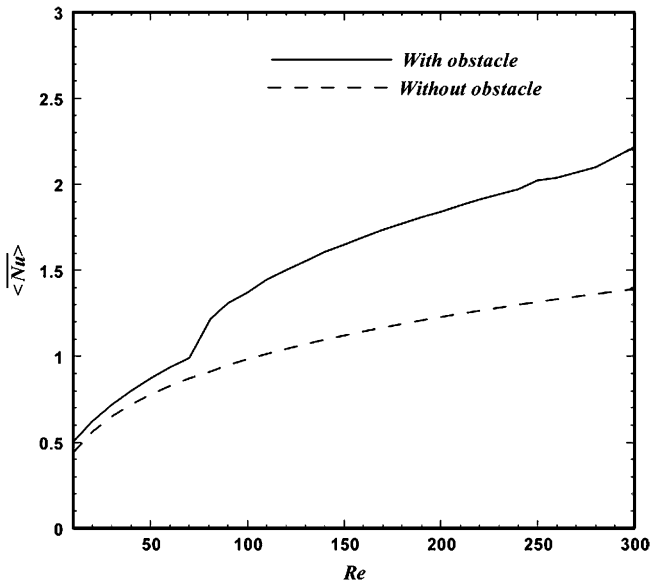

Fig. 14. Variation of the space- and time-averaged Nusselt number with the Reynolds number.

3.2.4. Average Nusselt number

The variation of the space- and time-averaged Nusselt numbers as function of the Reynolds number with and without the inclined square obstacle is plotted in Fig. 14. First, we can see that for every case, $\langle\overline{Nu}\rangle$ goes up largely when the Reynolds number increases. Two zones are distinguished: at relatively low Reynolds numbers corresponding to the symmetric flow ($Re \leq 80$), the presence of the obstacle has no significant effect in the space- and time-averaged Nusselt number. When the Reynolds number exceeds 80, the curves differ significantly. In other words, the presence of the inclined square cylinder leads to marked enhancement on the space- and time-averaged Nusselt number compared with that obtained without cylinder. At $Re = 300$ this augmentation is about 58%.

4. Conclusions

In this paper, the laminar flow of air and the heat transfer in a channel differentially heated and obstructed by an inclined square cylinder have been investigated by a 2-D hybrid scheme with lattice Boltzmann for fluid velocity fields and finite difference for temperature. The obtained results lead to the following conclusions:

- Even using a coarse mesh, the MRT-LBE captures the important physical phenomenon.
- The critical value of Reynolds number relative to transition from steady to periodic flow, for an inclined square prism inserted is about 82.
- For the symmetric flow ($Re < 82$), the presence of the inclined square prism has only local effects on the heat transfer and on the flow pattern, while for the periodic flow ($Re \geq 82$), the heat transfer is seen to increase strongly with *Re* in presence of the inclined square inner body.
- The drag coefficient shows a local minimum at $Re = 82$, also, the numerical method provides a local maximum of Strouhal number at $Re = 200$.
- The local Nusselt number changes only in the rear end of the inclined square prism due to the vortex shedding created by the presence of the obstacle.
- The averaged Nusselt number is an increasing function of the Reynolds number. The influence of the *Re* is more significant in the presence of the inclined square cylinder.
- The maximum enhancement of heat transfer is about 58% for $Re = 300$ in the presence of the inclined square cylinder. The increase in the apparent friction factor is also important.

References

[1] R.W. Davis, E.F. Moore, L.P. Purtell, A numerical-experimental study of confined flow around rectangular cylinders, Phys. Fluid. 27 (1) (1984) 46–59.
[2] T. Igarashi, Characteristics of the flow around a square prism, Bull. JSME 27 (231) (1984) 1858–1864.
[3] T. Igarashi, Heat transfer from a square prism to an air stream, Int. J. Heat Mass Transf. 28 (1) (1985) 175–181.
[4] G. Li, J.A.C. Humphrey, Numerical modelling of confined flow past a cylinder of square cross section at various orientations, Int. J. Numer. Meth. Fluid. 20 (11) (1995) 1215–1236.
[5] A. Sohankar, C. Norberg, L. Davidson, Low-Reynolds number flow around a square cylinder at incidence: study of blockage, onset of vortex shedding and outlet boundary conditions, Int. J. Numer. Meth. Fluid. 26 (1998) 39–56.
[6] S. Turki, H. Abbassi, S.B. Nasrallah, Two-dimensional laminar fluid flow and heat transfer in a channel with a built-in heated square cylinder, Int. J. Therm. Sci. 42 (12) (2003) 1105–1113.

[7] H. Abbassi, S. Turki, S. Ben Nasrallah, Numerical investigation of forced convection in a plane channel with a built-in triangular prism, Int. J. Therm. Sci. 40 (7) (2001) 649–658.
[8] A.K. De, A. Dalal, Numerical study of laminar forced convection fluid flow and heat transfer from a triangular cylinder placed in a channel, J. Heat Transf. 129 (5) (2007) 646–656.
[9] I. Ginzburg, F. Verhaeghe, D. d'Humières, Two-relaxation-time Lattice Boltzmann Scheme: about parametrization, velocity, pressure and mixed boundary conditions, Comm. Comput. Phys. 3 (2) (2008) 427–478.
[10] I. Ginzburg, F. Verhaeghe, D. d'Humières, Study of simple hydrodynamic solutions with the two-relaxation-times Lattice Boltzmann scheme, Comm. Comput. Phys. 3 (3) (2008) 519–581.
[11] S.Y. Chen, G.D. Doolen, Lattice Boltzmann method for fluid flows, Annu. Rev. Fluid Mech. 30 (1998) 329–364.
[12] A. Mezrhab, M.A. Moussaoui, H. Naji, Lattice Boltzmann simulation of surface radiation and natural convection in a square cavity with an inner cylinder, J. Phys. D Appl. Phys. 41 (2008) 115502.
[13] E. Semma, M. El Ganaoui, R. Bennacer, A.A. Mohamad, Investigation of flows in solidification by using the lattice Boltzmann method, Int. J. Therm. Sci. 47 (3) (2008) 201–208.
[14] M. Cheng, S.H.N. Tan, K.C. Hung, Linear shear flow over a square cylinder at low Reynolds number, Phys. Fluid. 17 (2005) 078103.
[15] L. Zhou, M. Cheng, K.C. Hung, Suppression of fluid force on a square cylinder by flow control, J. Fluid. Struct. 21 (2005) 151–167.
[16] M. Breuer, J. Bernsdorf, T. Zeiser, F. Durst, Accurate computations of the laminar flow past a square cylinder based on two different methods: lattice-Boltzmann and finite-volume, Int. J. Heat Fluid Flow 21 (2000) 186–196.
[17] Z. Guo, H. Liu, L.S. Luo, K. Xu, A comparative study of the LBE and GKS methods for 2D near incompressible laminar flows, J. Comput. Phys. 227 (2008) 4955–4976.
[18] W.-B. Guo, N.-C. Wang, B.-C. Shi, Z.-L. Guo, Lattice-BGK simulation of a two-dimensional channel flow around a square cylinder, Chin. Phys. 12 (1) (2003) 67–74.
[19] P. Lallemand, L.-S. luo, Theory of the lattice Boltzmann method: acoustic and thermal properties in two and three dimension, Phys. Rev. E 68 (3) (2003) 036706.
[20] P. Lallemand, L.-S. luo, Hybrid finite-difference thermal lattice Boltzmann equation, Int. J. Mod. Phys. B 17 (1/2) (2003) 41–47.
[21] A. Mezrhab, M. Bouzidi, P. Lallemand, Hybrid lattice Boltzmann finite-difference simulation of convective flows, Comput. Fluid. 33 (2004) 623–641.
[22] P.V. Leemput, C. Vandekerckhove, W. Vanroose, D. Roose, Accuracy of hybrid Lattice Boltzmann/finite difference schemes for reaction-diffusion systems, Mutiscale Model. Simul. 6 (3) (2007) 838–857.
[23] C.V. Treeck, E. Rank, M. Krafczyk, J. Tolke, B. Nachtwey, Extension of a hybrid thermal LBE scheme for large-eddy simulations of turbulent convective flows, Comput. Fluid. 35 (2006) 863–871.
[24] U. Frisch, D. Hasslacher, Y. Pomeau, Phys. Rev. Lett. 56 (1986) 1505–1508.
[25] P.L. Bhatnagar, E.P. Gross, M. Krook, A model for collision processes in gases. I. Small amplitude processes in charged and neutral one-component systems, Phys. Rev. 94 (1954) 511–525.
[26] P. Lallemand, L.-S. Luo, Theory of the lattice Boltzmann method: dispersion, dissipation, isotropy, Galilean invariance, and stability, Phys. Rev. E 61 (2000) 6546–6562.
[27] I. Ginzburg, D. d'Humières, Multireflection boundary conditions for lattice Boltzmann models, Phys. Rev. E 68 (2003) 066614.
[28] D. d'Humières, Generalized lattice Boltzmann equations, in: B.D. Shizgal, Weaver (Eds.), Rarefied Gas Dynamics: Theory and Simulations, Prog. Aeronaut. Astronaut 159 (1992) 450–458.
[29] M. Bouzidi, M. Firdaouss, P. Lallemand, Momentum transfer of a Boltzmann-lattice fluid with boundaries, Phys. Fluid. 13 (11) (2001) 3452–3459.
[30] I. Ginzburg, P.M. Adler, Boundary flow condition analysis for the three dimensional lattice Boltzmann model, J. Phys. II France 4 (1994) 191–214.
[31] P. Lallemand, L.-S. Luo, Lattice Boltzmann method for moving boundaries, J. Comput. Phys. 184 (2003) 406–426.
[32] M. Jami, A. Mezrhab, M. Bouzidi, P. Lallemand, Lattice-Boltzmann computation of natural convection in a partitioned enclosure with inclined partitions attached to its hot wall, J. Comput. Phys. 368 (2) (2006) 481–494.
[33] R. Kahawita, P. Wang, Numerical simulation of the wake flow behind trapezoidal bluff bodies, Comput. Fluid. 31 (1) (2002) 99–112.
[34] A.K. De, A. Dalal, Numerical simulation of unconfined flow past a triangular cylinder, Int. J. Numer. Meth. Fluid. 52 (2006) 801–821.
[35] A. Okajima, Strouhal numbers in rectangular cylinders, J. Fluid Mech. 123 (1982) 379–398.